



OPEN

Influence of *Pholiota adiposa* on gut microbiota and promote tumor cell apoptosis properties in H22 tumor-bearing mice

Xiao-yan Wang^{1,2}, Ying Zhang¹ & Fang-fang Liu²✉

Hepatocellular carcinoma (HCC) is a common type of cancer—prevalent worldwide—and one of the causes of cancer-related deaths. In this study, ethanol extracts from *Pholiota adiposa* (EPA) were used to identify possible targets for HCC treatment and their effects on intestinal microflora were analyzed. **Methods:** Male mice were randomly assigned to groups—the model group, cyclophosphamide (25 mg/kg/d), and EPA groups, in which the mice were categorized based on the different concentrations of each compound (100, 200, and 300 mg/kg/day). Relevant biochemical indicators were detected using ELISA, H&E staining, and TUNEL assay. Four tumor apoptosis-related proteins and genes, Cleaved Caspases, *BAX*, *Bcl-2*, and *VEGF*, were detected by immunohistochemical staining, western blotting, and RT-PCR. The total genomic DNA was obtained from the contents of the small intestine and colon and was sequenced. The V3 + V4 regions of bacterial 16 s rDNA (from 341 to 806) were amplified. **Results:** The tests revealed that EPA exhibited antitumor activity *in vivo* by promoting apoptosis and inhibiting angiogenesis. Moreover, EPA treatment could increase beneficial and decrease harmful microflorae. These results demonstrate that EPA may be a potential therapy for HCC.

The incidence of liver cancer is high worldwide, with the highest observed morbidity and mortality rates. The incidence of liver cancer has decreased in developed countries, while it continues to increase in developing countries². The currently available treatment routes for cancer include surgery, radiotherapy, and chemotherapy, but the efficiency of these treatments is low and they have various adverse effects³. Therefore, it is necessary to develop or discover new low toxicity drugs for cancer treatment. The mouse hepatocellular carcinoma (HCC) cell line H22 is used extensively to establish an animal tumor model⁴, and cyclophosphamide (CTX) is mostly used as the positive control drug to investigate the antitumor effects of bioactive compounds⁵.

Drug therapy is a conventional strategy against cancer, and there are several antitumor drugs available in the market, such as CTX, paclitaxel, and oxaliplatin. Although chemotherapeutic drugs have good tumor inhibiting properties, they also have significant side effects, such as dysfunction of other organs or gastrointestinal problems⁶. Natural sources, especially medicinal fungi, may be considered as potential hypoglycemic agents because of their high efficacy, and low toxicity.

Pholiota adiposa is a famous edible mushroom found in Northeast Asia, and its fruit body has a better anti-tumor effect. *P. adiposa* is rich in polysaccharides, proteins, vitamins, and sterols⁷. The fruit body of *P. adiposa* is rich in medicinal properties and contains functional substances, such as polysaccharides, peptides, polyunsaturated fatty acids, ribonucleic acids, lectins, triterpenoids, adenine, and steroids⁸. Consumption of *P. adiposa* has potential benefits, including heat dissipation, and promotion and regulation of the human body⁹.

The relationship between intestinal microorganisms and the occurrence and development of diseases has attracted considerable attention. In the human body, the gut microbiota has important functions in metabolism, digestion, and intestinal barrier protection⁹. At present, development of molecular biology technologies, which affect intestinal microorganisms, has attracted the attention of researchers. And maintain the stability of the gut internal environment of the organism^{9–11}, where in the relatively stable structure of the gut microbiota is of great significance to human health. Several factors affect the diversity of gut microbiota, such as obesity, diabetes, irritable bowel syndrome, and cancer^{9,12}. In addition, antibiotic use and diet also have certain effects on the diversity of the gut microbiota^{9,13}. Increasing evidence indicates that aberrant gut microbiota has a profound

¹Academy of Traditional Chinese Medicine, Jilin Agricultural Science and Technology University, Jilin, China. ²Academy of Medical, Changchun Sci-Tech University, Changchun, China. ✉email: liuff_1981_2006@163.com

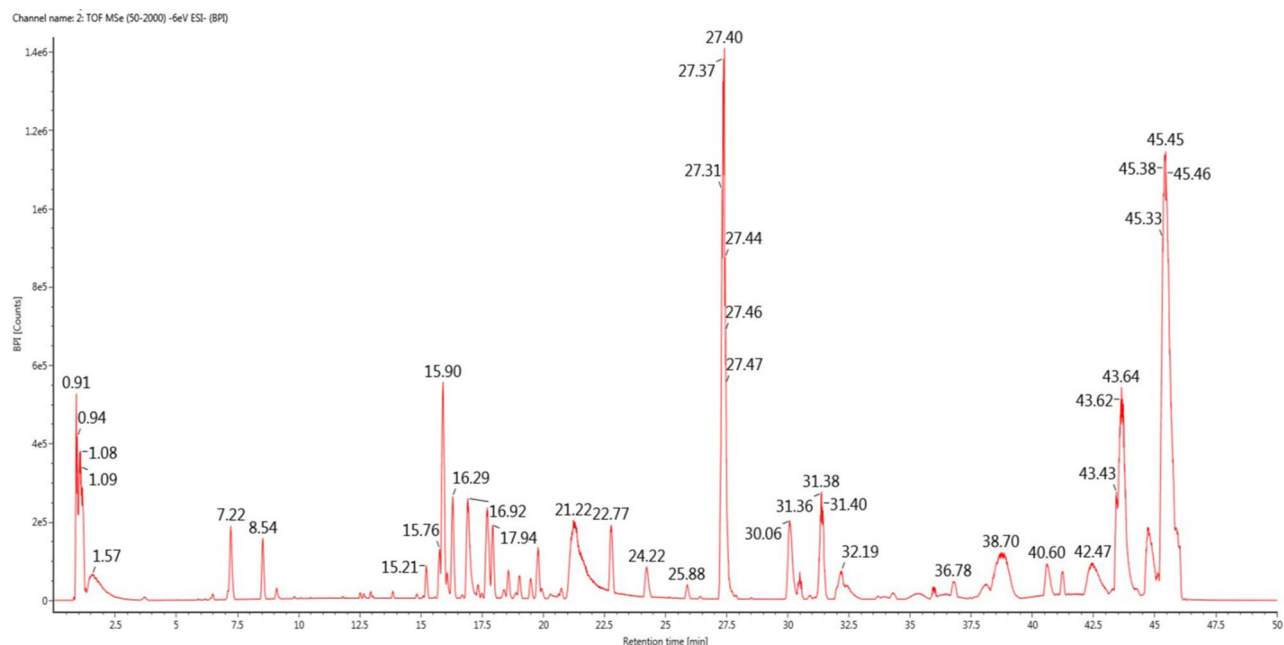


Figure 1. The total ion chromatogram of the extracted of *Pholiota adiposa* detected by LS-MS.

RT (min)	CAS number	Component name	Chemical formula	Expected mass (Da)	Observed m/z	Mass error (mDa)	Percentage (%)
27.31	2061-64-5	Ergosterol peroxide	C ₂₈ H ₄₄ O ₃	428.32905	427.31985	-0.51	0.799
27.40	19,254-69-4	Ergosta-4,6,8(14)22,-tetraen-3-one	C ₂₈ H ₄₀ O	392.30792	391.29748	-0.71	0.3256
27.46	57-87-4	Ergosterol	C ₂₈ H ₄₄ O	396.64805	395.42196	-0.82	0.35
30.06	14,858-07-2	(22E,24R)-ergosta-7,22-dien-3 β ,5 α ,6 β -triol	C ₂₈ H ₄₆ O ₃	430.34471	465.31065	-1.45	0.158

Table 1. Affiliation of key peaks of EPA.

impact on the onset and progression of cancer development; therefore, understanding the diversity of bacterial flora in feces can help understand the changes in disease⁹.

Previous research has shown that *P. adiposa* has a good antitumor effect⁸. In this study, ethanol extract from the fruit body of *P. adiposa* (EPA) was obtained and analyzed using LS-MS liquid mass spectrometry to demonstrate the antitumor activity of EPA in an H22 tumor-bearing mouse model. We investigated the possible molecular mechanisms underlying the antitumor action of EPA. Additionally, we also investigated the influence of EPA on gut microbiota using feces of tumor-bearing mice and compared it with that of the normal control group, model group, and EPA control group mice.

Results

The results of LC-MS analysis. As shown in Fig. 1, in the present study, under optimal chromatographic and MS conditions^{14,15}, 3 compounds were identified by comparing the retention times and matching the empirical molecular formulas with those of known saponins; six phenolic compounds, seven fatty acid compounds, three nucleotide compounds, five quinone compounds, six carbohydrate compounds, and four steroid compounds were identified, and sterol compounds, such as ergosterol peroxide, ergosta-4, 6, 8(14)22-tetraen-3-one, ergosterol, and (22E,24R)-ergosta-7, 22-dien-3 β ,5 α ,6 β -triol, accounted for a high proportion (Table 1).

Analyses of tumor weight, tumor inhibitory rate, and organ index. The tumor volume growth curves are shown in Fig. 2. The tumor growth rate in the model group was more than 2.6 cm³ on Day 15. In contrast, CTX-treated and all EPA-treated groups showed obvious inhibition of tumor growth.

The organ index, tumor weight, and tumor inhibitory rate (TIR) are shown in Table 2. The CTX-treated group exhibited the highest TIR (92.42%). Moreover, the tumor weight in the EPA-treated groups significantly decreased in a dose-dependent manner, with tumor inhibitory rates of 79.70%, 84.55%, and 87.28%. The spleen and thymus indices were significantly lower in the CTX-treated group than in the normal group, and the thymus was severely atrophic ($p < 0.05$). The EPA-treated groups showed significant improvements, and there was a protective effect on the spleen and thymus.

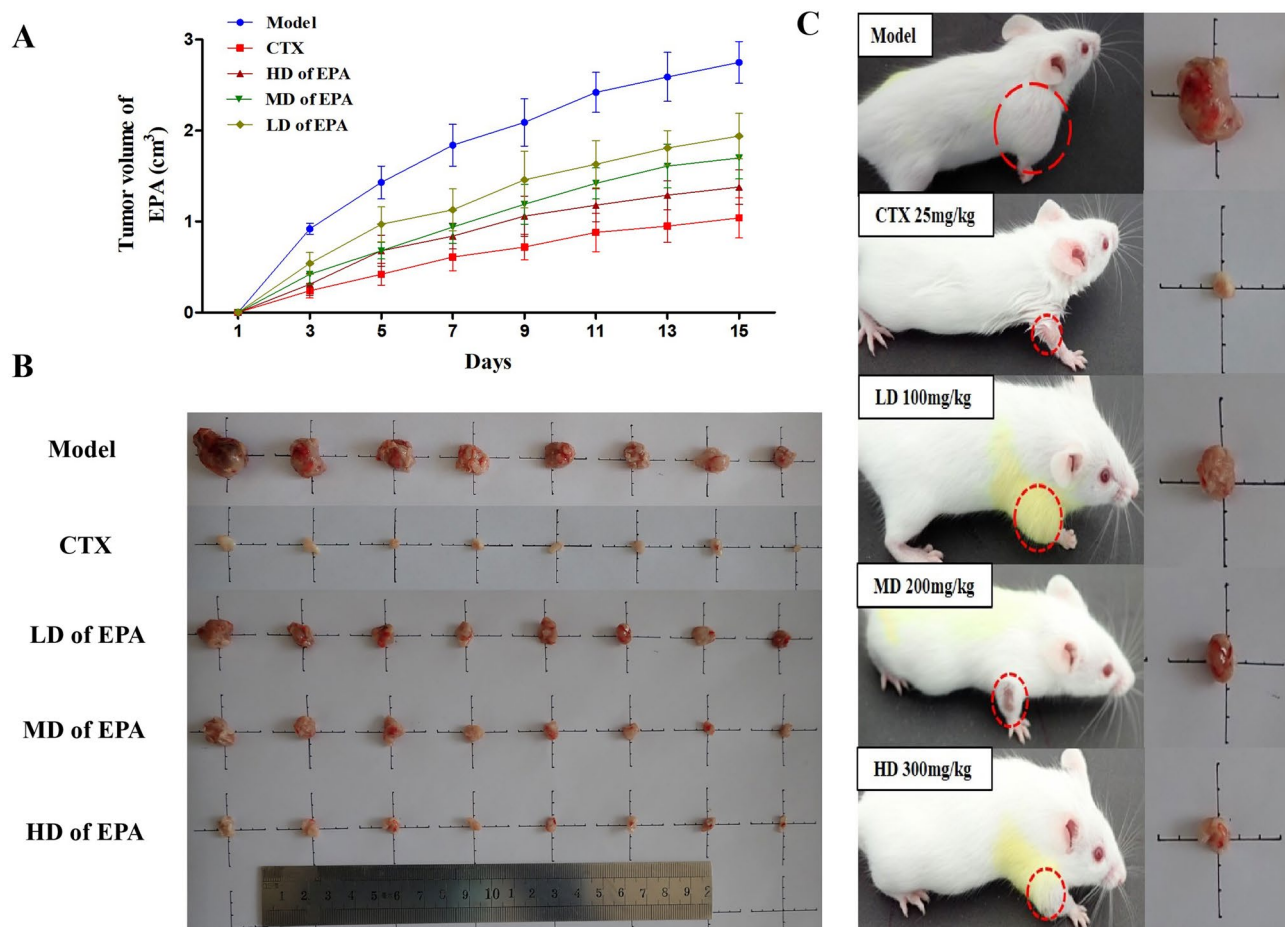


Figure 2. The effects of EPA on tumor H22 tumor-bearing mice.

Groups	Dose	Organ index (%)		Tumor weight (g)	Tumor Inhibitory rate (%)
		Thymus	Spleen		
Normal		5.75 ± 1.12**	5.62 ± 1.95**	–	–
Model		4.16 ± 1.37	10.86 ± 1.47##	3.30 ± 0.72	–
CTX	25mg/kg	2.42 ± 0.48***	2.73 ± 1.24***	0.25 ± 0.12**	92.42%
LD of SLM	100 mg/kg	4.93 ± 1.25**	8.63 ± 1.31***	0.67 ± 0.25**	79.70%
MD of SLM	200 m g/kg	4.87 ± 0.94**	7.54 ± 1.09***	0.51 ± 0.18**	84.55%
HD of SLM	300 mg/kg	4.58 ± 1.19*	6.73 ± 1.36**	0.42 ± 0.13**	87.28%

Table 2. Effect of EPA on tumor weights and tumor inhibition rate. The values are presented as mean ± SD. n = 10, *p < 0.05, **p < 0.01 compared with the Normal group, #p < 0.05, ##p < 0.01 compared with the Model group.

Analysis of the expression of serum cytokines and VEGF in mice. ELISA was used to investigate the effects of EPA on serum cytokine production, including TNF- α , IFN- γ , IL-2, AST, BUN, and IL-6, in H22 tumor-bearing mice. Angiogenesis has become an important therapeutic target for many tumors and is an essential process for tumor growth and metastasis^{10,16}.

As shown in Fig. 3, compared with the levels in the normal and model groups, the serum levels of IL-2, IL-6, IFN- γ , and TNF- α significantly increased in the EPA-treated HD group ($p < 0.05$). VEGF levels were significantly decreased in the CTX-treated and EPA-treated groups. The AST and BUN levels in the model group were significantly higher than those in the normal control group ($p < 0.05$). The values of these two parameters significantly decreased in the EPA-treated groups compared to those in the model control group ($p < 0.05$). The AST levels of mice in the CTX-treated group were significantly higher than those of the model group ($p < 0.05$).

Morphological analysis after treatment with EPA. Histopathology was evaluated using hematoxylin and eosin (H&E) staining of the tumor. As shown in Fig. 4A, tumor cell in the model group were plump and

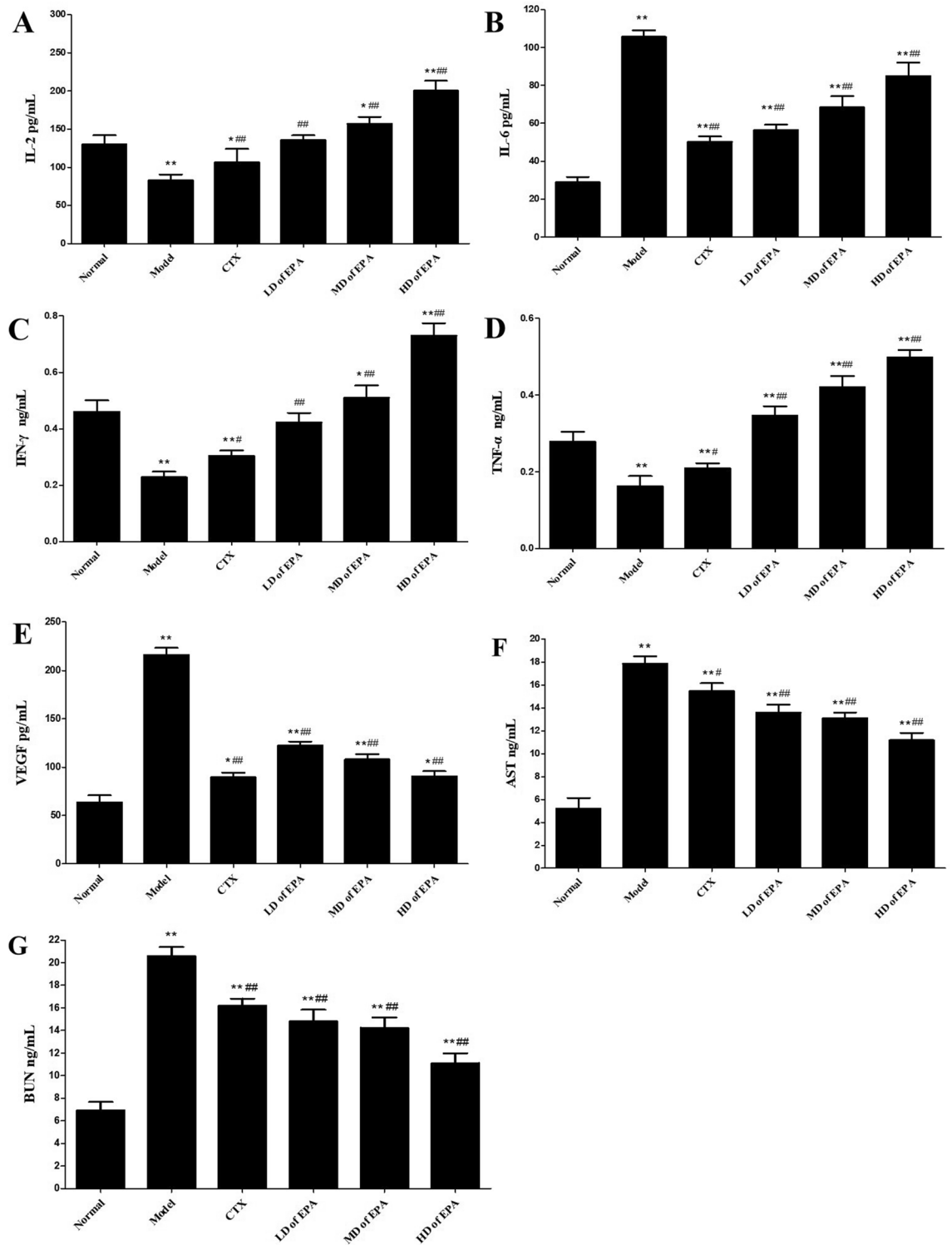


Figure 3. Effects of EPA on levels of serum cytokines, including, IL-2 (A), IL-6 (B), IFN-γ (C), TNF-α (D), VEGF (E), AST (F) and BUN (G).

intact, with large nuclei. After treatment with EPA and CTX, the tumor cells exhibited a large necrotic region and were stained darker, which indicates that the significant antitumor efficacy of EPA in H22 tumor-bearing mice involved inducing cell death.

The TUNEL assay results are shown in Fig. 4B,C, and cells with brown granules were considered positively stained^{10,17}. The percentage of positive cells in the model group was 5%; therefore, the amount of tumor cell apoptosis was minimal. However, the CTX-treated group exhibited the highest percentage of positive cells (44%). The EPA-treated groups showed an increase in the number of cells undergoing apoptosis, with values of 12%,

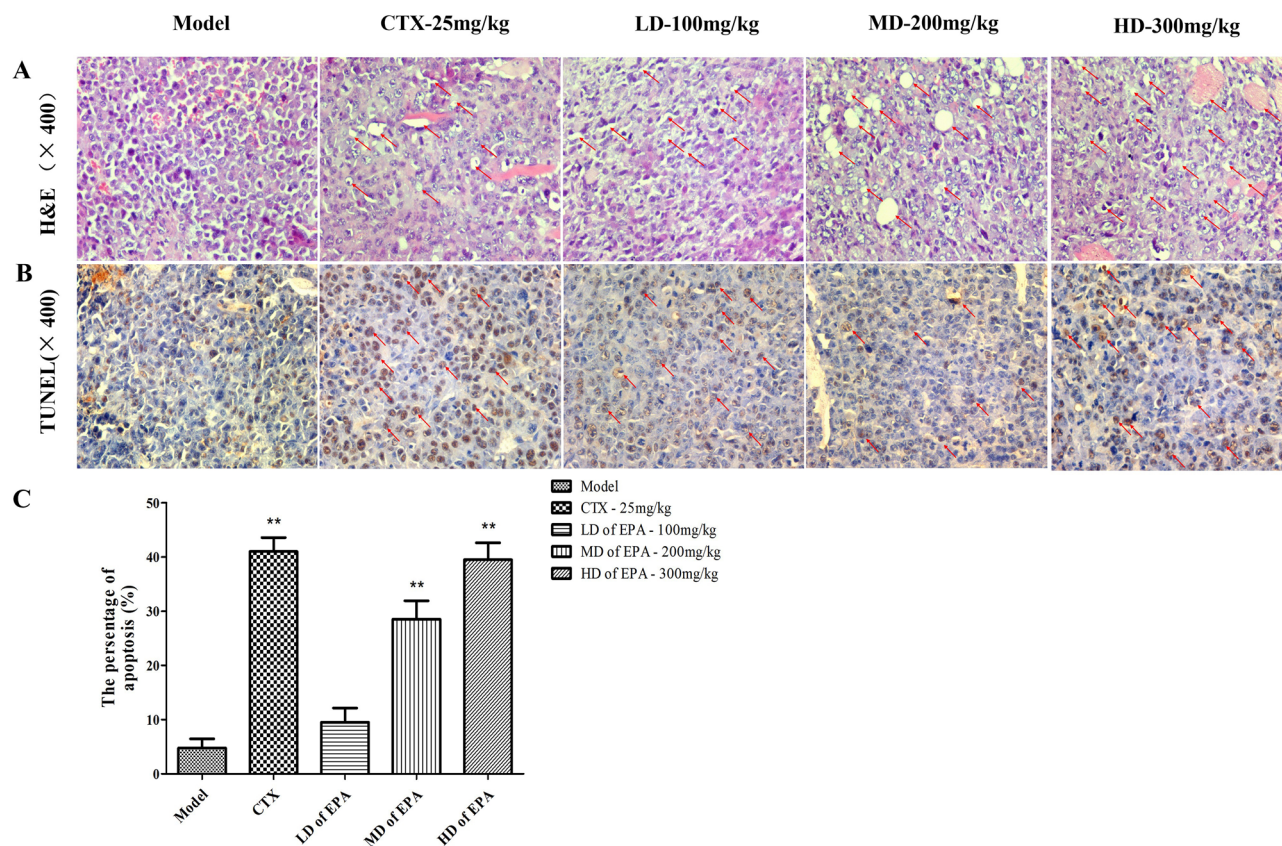


Figure 4. Histological examination of the morphological changes in tumors from H22-bearing mice. Tumor tissues stained with H&E (A) (400 \times) TUNEL assay (400 \times) (B,C).

28%, and 42%. Moreover, the mice in the HD and EPA-treated group showed a positive cell percentage similar to that of the CTX-treated group.

Effects of EPA on the expression of apoptosis-related proteins and VEGF. Based on the results of previous studies¹⁸, immunohistochemical analysis was performed on the proapoptotic factor BAX, the anti-apoptotic factor Bcl-2, and cleaved caspase 3 to determine the expression of apoptosis-related proteins, as shown in Fig. 5. BAX and cleaved caspase 3 expression intensities increased, while Bcl-2 expression decreased in the EPA-treated groups in a dose-dependent manner. Therefore, the ratio of Bcl-2 to BAX decreased significantly. The vascular endothelial growth factor (VEGF) level in the EPA-treated groups significantly decreased in a dose-dependent manner, and VEGF expression was lowest in the CTX-treated group.

In addition, western blotting was used to analyze the expression of Bcl-2, BAX, cleaved caspase 3, and VEGF. As shown in Fig. 6, all EPA-treated groups showed increased BAX and cleaved caspase 3 protein expression and decreased Bcl-2 and VEGF protein expression; these results were consistent with the results of the immunohistochemical analysis. However, the expression of PI3K/AKT and p-AKT/AKT increased in a dose-dependent manner in the EPA-treated group.

Results of the rank-abundance curves of microorganisms in samples. The rank-abundance curve is a method used to analyze the diversity of microorganisms. In this study, the operational taxonomic unit (OTU) rank-abundance curves showed the diversity in the samples, which can be explained by species richness and evenness¹⁹. In the horizontal direction, the wider the span of the curve is, the richer the species rank of the microorganism sample²⁰. The OTU rank-abundance curve in this study showed that the abundance distribution of the samples was even, as it was flat and smooth in the vertical direction (Fig. 7). The richness and evenness of the samples shown in the rank-abundance curve indicate that the diversity of the samples was rational and reasonable.

Dilution curves of microorganisms in the gut microbiota. The dilution curve was used to evaluate whether the sample sequencing depth was sufficient to cover all species of microbes and compare species richness among different sequenced samples. A flat curve indicates that the sequencing data are reasonable and reflect the structure of the entire community²¹. The number of sequences reached 5000, and the curves were in the plateau stage (Fig. 8). Therefore, the experimental data were deemed reasonable and reliable.

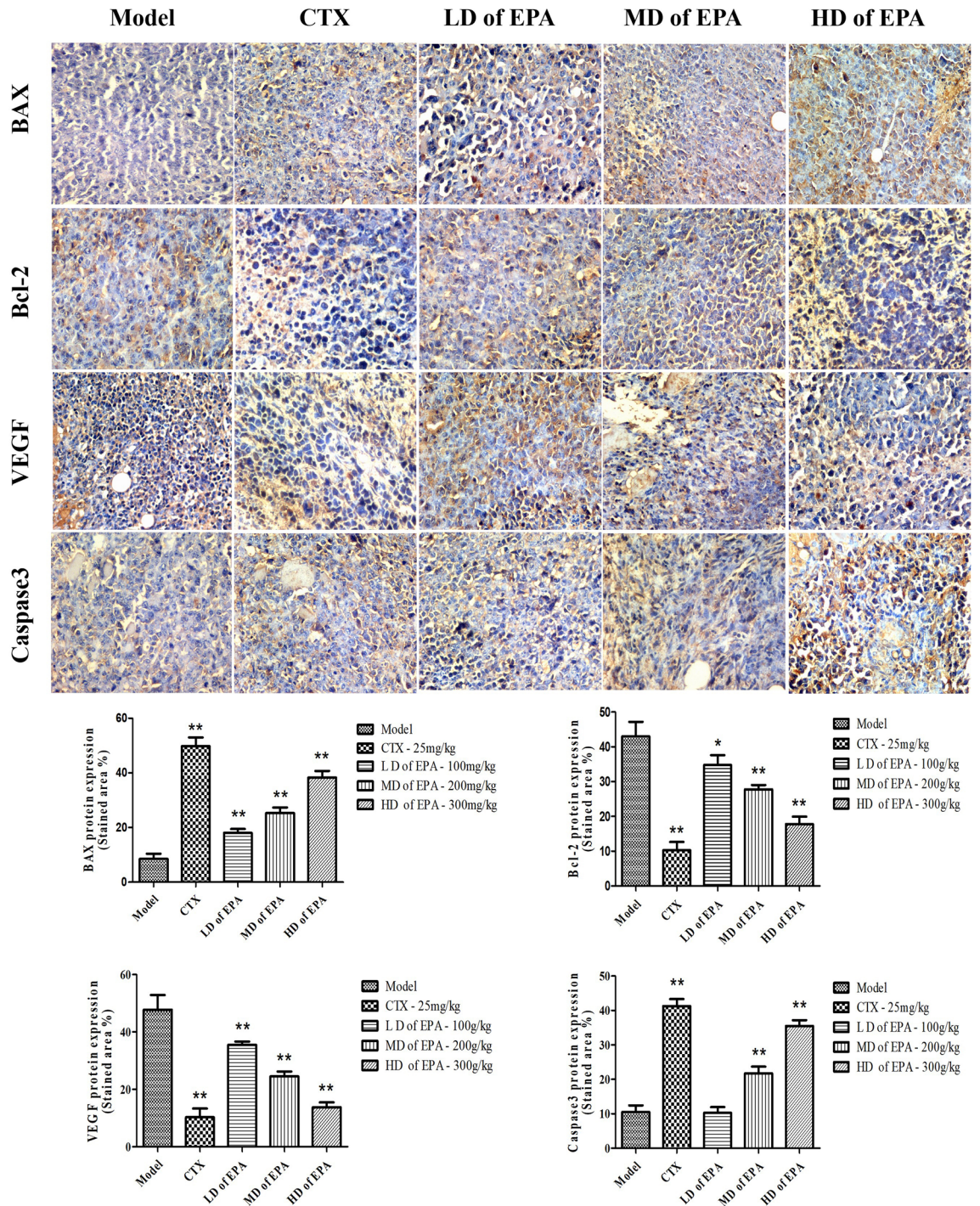


Figure 5. Immunohistochemical analysis of tumor tissues and stained area of tumor tissues.

Species accumulation curves of the gut microbiota. The species accumulation curve is used to describe the increase in species with the increase in the number of samples and is an effective tool for investigating the composition and predicting the abundance of species in samples. This curve reflects whether the number of samples was sufficient. In this study, we mainly observed the end of the curve; if it showed a sharp upward trend, the number of samples was considered insufficient, while if the end of the curve tended to be flat, the number of samples was considered sufficient²². The end of the species accumulation curves of Specaccums tended to be flat in this study; therefore, the sampling was considered sufficient to carry out data analysis (Fig. 9).

Results of alpha diversity analysis of the gut microbiota. In this study, six indicators, including the Chao1 index, observed species index, PD_whole_tree index, goods-coverage index, Shannon index, and Simp-

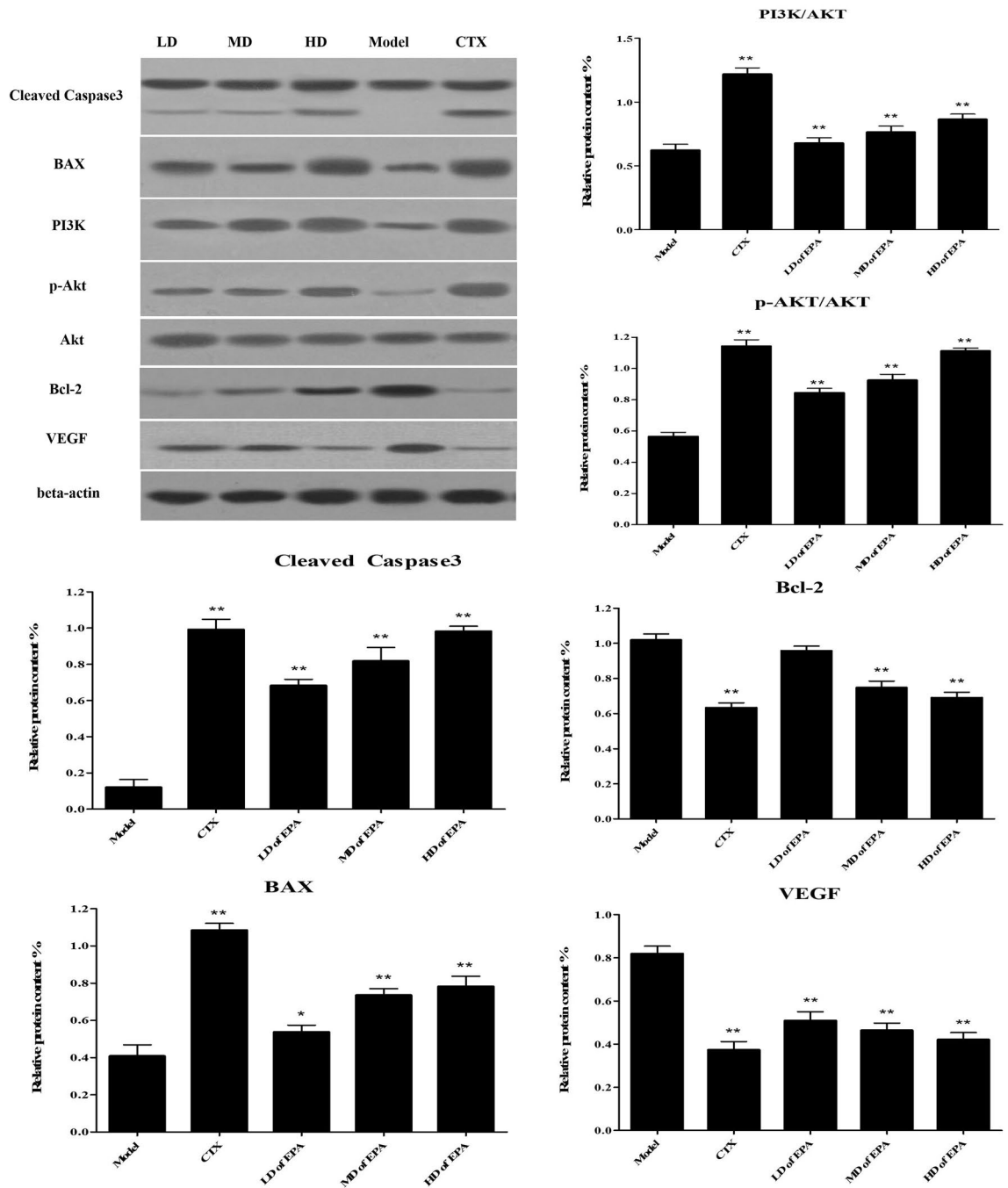


Figure 6. Relative protein expression of BAX, Bcl-2, Caspase3, AKT, p-AKT,PI3K and VEGF in tumor tissue.

son’s index, were analyzed to assess the species diversity of individual samples (Fig. 10). There was no significant difference in flora abundance or diversity between the normal, model, and HD groups in the EPA-treated group.

Results of beta diversity analysis of the gut microbiota. Beta diversity analysis was used to compare the differences in species diversity among intergroup samples, and the evolutionary distance between species was considered while calculating the results. The higher the index value, the greater the difference between the samples. In this study, the UniFrac results were divided into two parts: the weighted UniFrac, which considered the abundance of the sequence, and the unweighted UniFrac, which did not consider the abundance of the sequence. According to the statistical analysis of the differences of the clustered samples, the similarity of species composition among the samples was determined by calculating the distance between the samples²³.

ANOSIM similarity analysis was used to determine the intergroup and intragroup differences, and the grouping was found to be meaningful (Fig. 11). The R value of the unweighted results was $R = 0.34 > 0$ and $p = 0.001 < 0.05$, indicating that the differences between the groups were significantly greater than those within

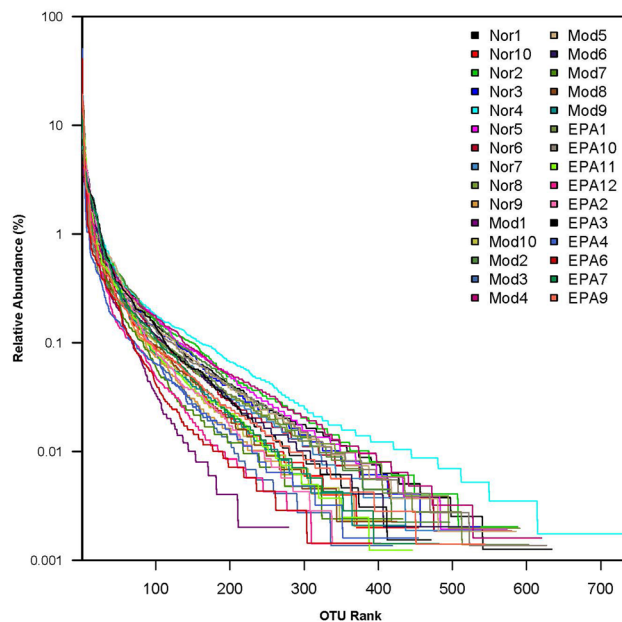


Figure 7. OTU Rank-Abundance curves. Different samples are represented by curves of different colors. The abscissa is the number rank sorted by OTU abundance, and the ordinate is the corresponding OTU abundance.

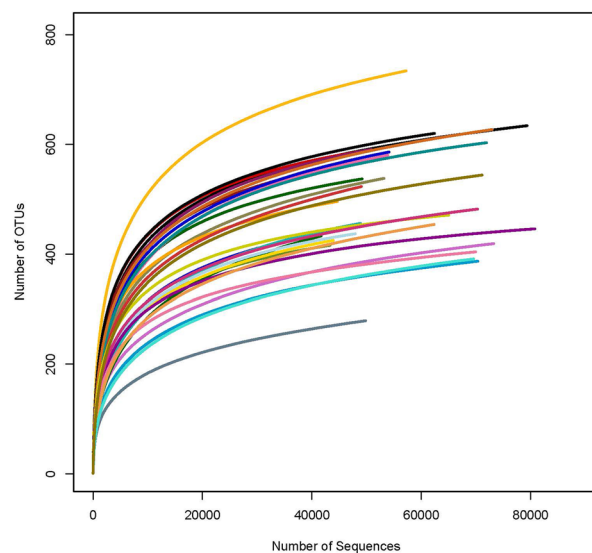


Figure 8. Dilution curve of the alpha diversity index for species abundance of samples. The horizontal axis represents the number of clean reads randomly extracted from a sample, and the vertical axis represents the alpha.

the group (intragroup). Therefore, the result is reasonable, and the data are statistically significant. Thus, in this study, the gut microbiota in tumor-bearing mice tended to be normal after EPA treatment.

Principal coordinates analysis (PCoA) was used to evaluate the differences between samples (Fig. 12)²⁴. If the samples were in close proximity, the species compositions of the samples were similar. The EPA-treated group was closer in distance to the normal group, indicating that both groups had similar gut microbiotas.

Difference Analysis of the Gut Microbiota. To emphasize the statistical significance and biological relevance, the LEfSe analysis of the gut microflora was performed, and the results are presented quantitatively in an LDA Score column and a cladogram. This study aimed to estimate the impact of the abundance of each component and identify the significant difference effect on the division of samples²³. The results showed significant differences in the gut microflora, such as *Lactobacillus*, *Streptococcus*, *Streptococcaceae*, *Rikenellaceae*, *Alistipes* (Nor), *Campylobacterales*, *Epsilonproteobacteria*, *Helicobacteraceae*, *Helicobacter*, *Escherichia_Shigella*,

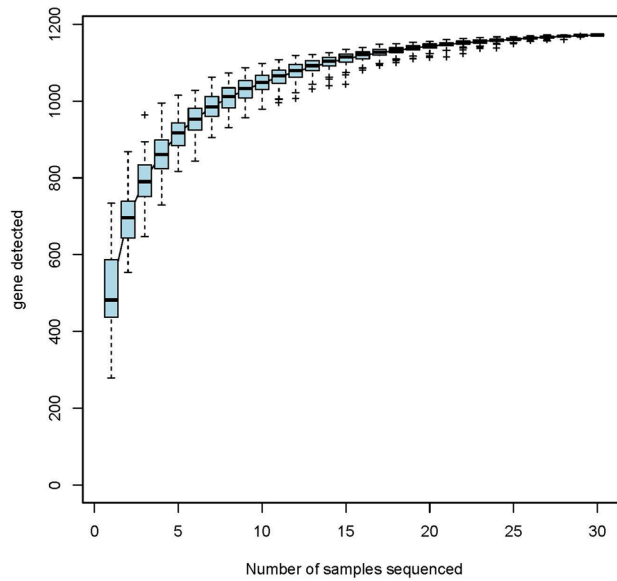


Figure 9. Species accumulation curves. Abscissa sample size ordinate OTU number after sampling.

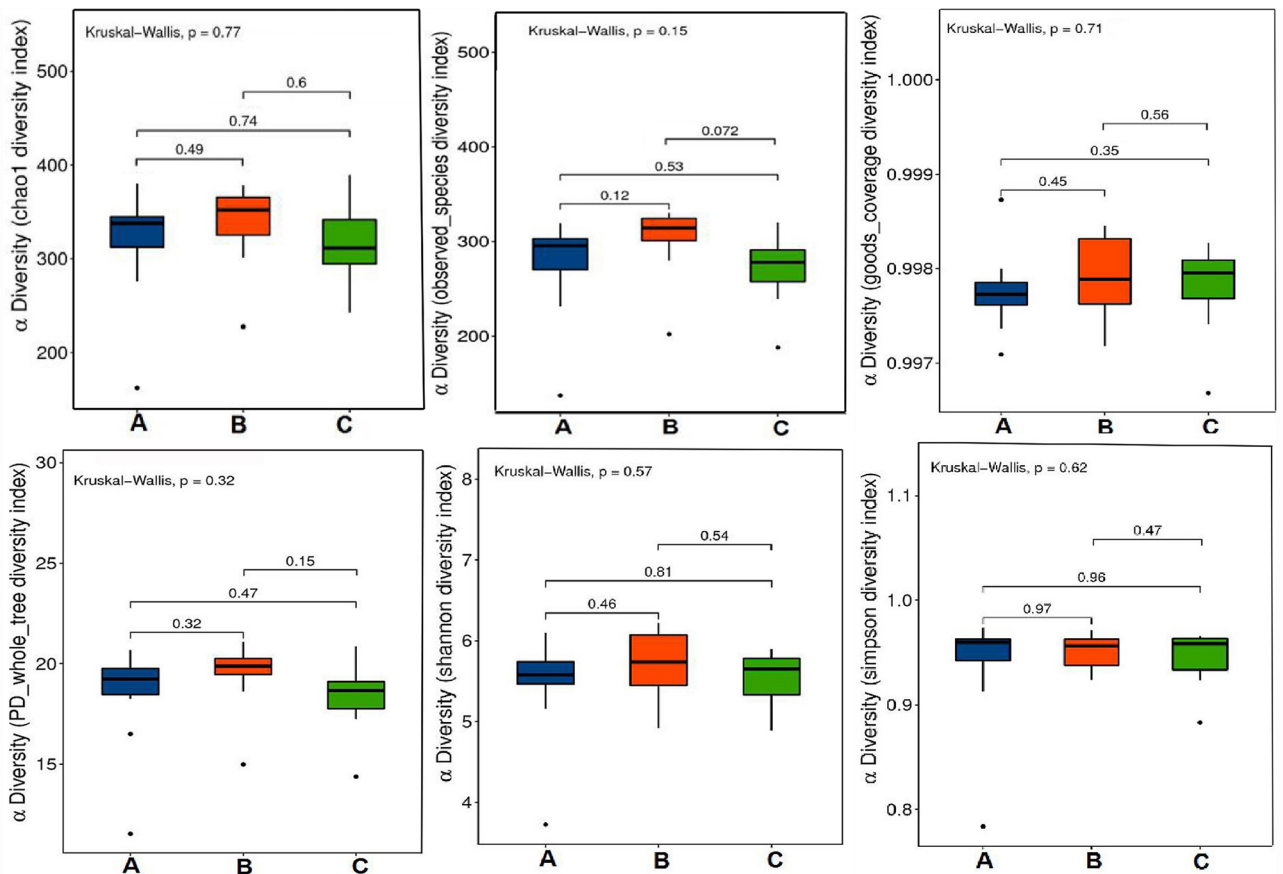


Figure 10. Alpha-diversity boxplots in Normal group, Model group and HD of SLM group, such as Chao1 (a), Observed (b), Goods_coverage (c), PD_whole_tree (d), Shannon (e), and Simpson indexes (f).

Subdoligranulum (Mod), *Prevotellaceae*, *Proteobacteria*, *Bacteroidaceae*, *Bacteroides*, and *Selenomonadales* (EPA) (Figs. 13 and 14).

Species abundance in the gut microbiota. Histograms showing species profiling in the gut microflora of each sample were used to identify the species with higher relative abundances and individual samples at dif-

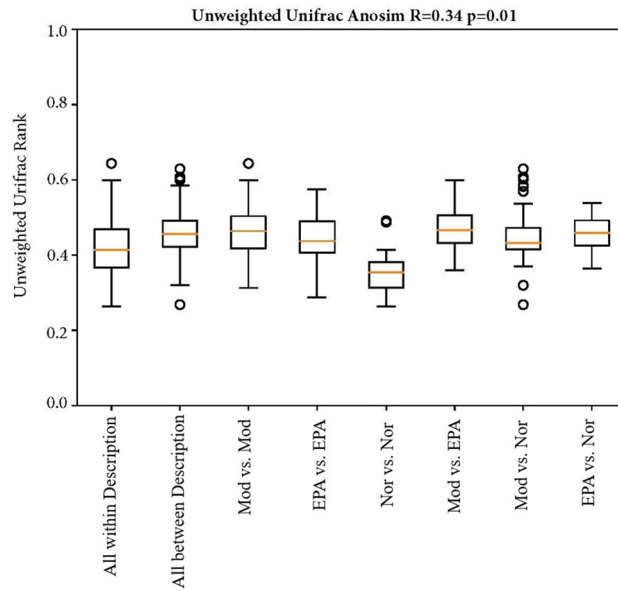


Figure 11. Anosim analysis of gut microbiota based on unweighted unifrac distance.

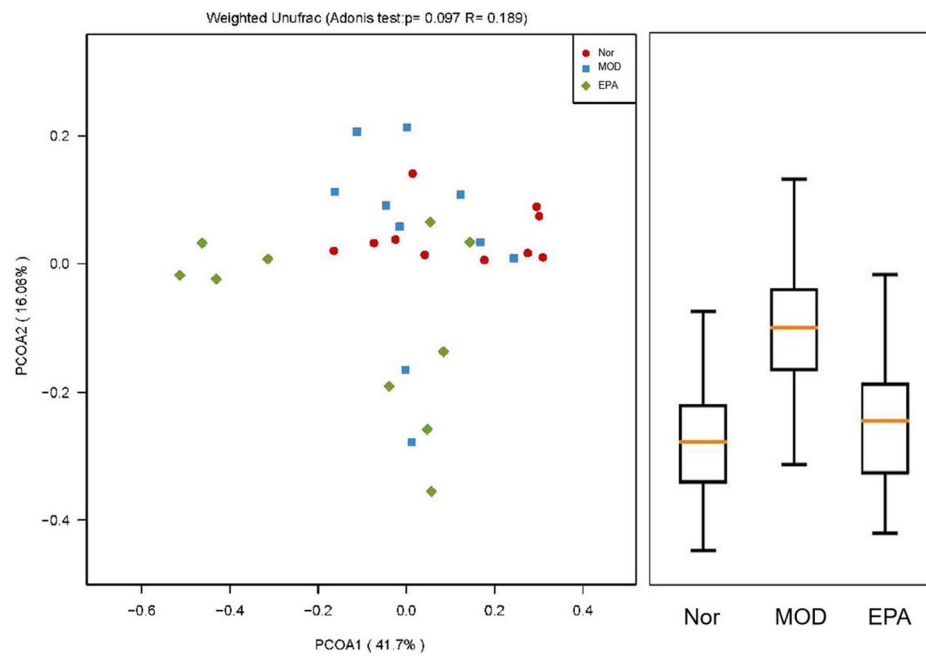


Figure 12. Principal coordinates analysis (PCoA) analysis of gut microbiota based on Weighted Unifrac distance. It illustrated the difference in the microbial composition among the samples.

ferent classification levels (Fig. 15A and Table 3)²⁵. In this study, the phylum level showed that *Firmicutes*, *Bacteroides*, and *Proteobacteria* accounted for more than 98% of the total microflora after the different treatments. Compared with that in the normal group, the abundance of *Bacteroidetes* and *Firmicutes* decreased, but *Proteobacteria* increased in the model group. In contrast, the abundance of *Bacteroidetes* and *Firmicutes* increased, but *Proteobacteria* decreased in the EPA-treated group and was close to that in the normal group. Thus, the trend in the two phyla in the microflora in the EPA-treated group trended more toward that in the normal group.

Figure 15B shows the genus level of the gut microflora in the three groups. Based on abundance, the main groups were *Lactobacillus*, *Bacteroidales_S24-7_group_norank*, *Bacteroidales*, *Lachnospiraceae_NK4A136_group*, *Prevotellaceae_UCG-001*, *Alloprevotella*, *Streptococcus*, *Alistipes*, *Prevotellaceae_UCG-003*, and *Helicobacter*. Based on the changing trend in the abundance of the gut microflora, it can be concluded that tumor-bearing mice that were treated with EPA tended to be closer to those in the normal control group. Compared with that in the

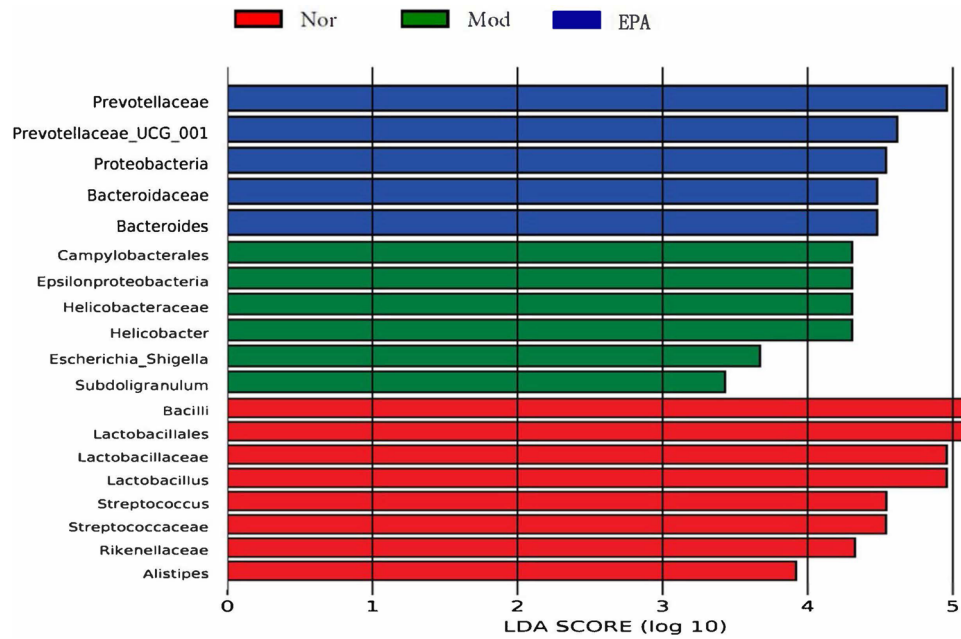


Figure 13. The LDA score obtained from LEfSe analysis of gut microbiota in different groups.

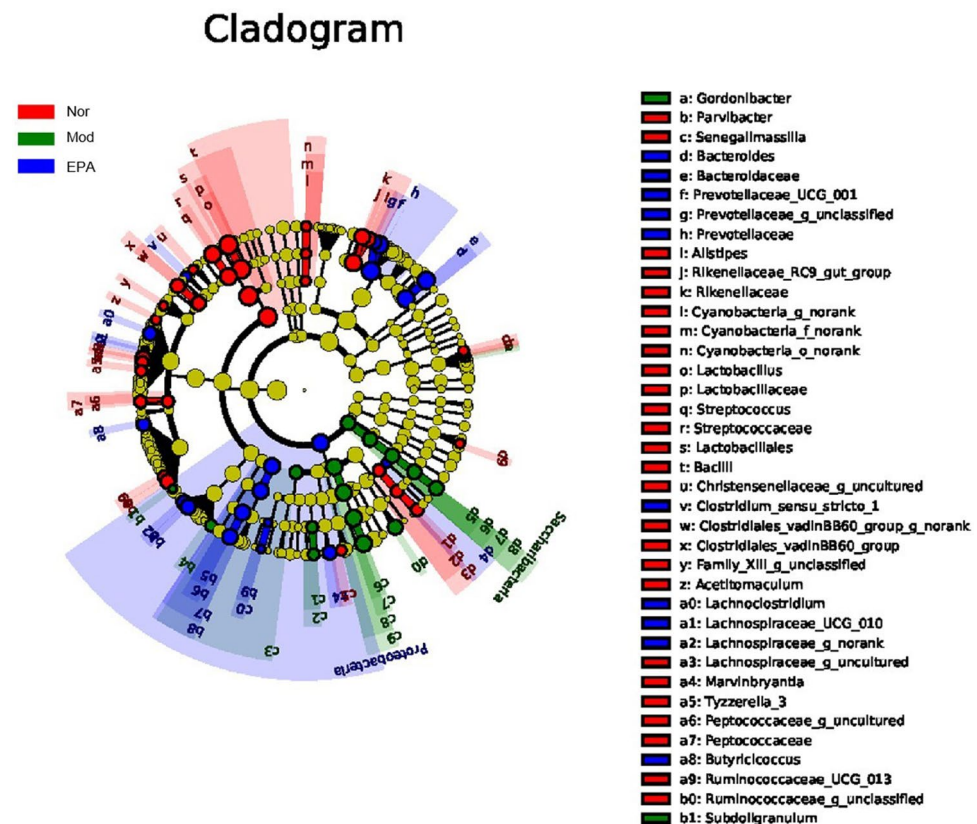


Figure 14. The LDA score obtained from LEfSe analysis of gut microbiota in different groups.

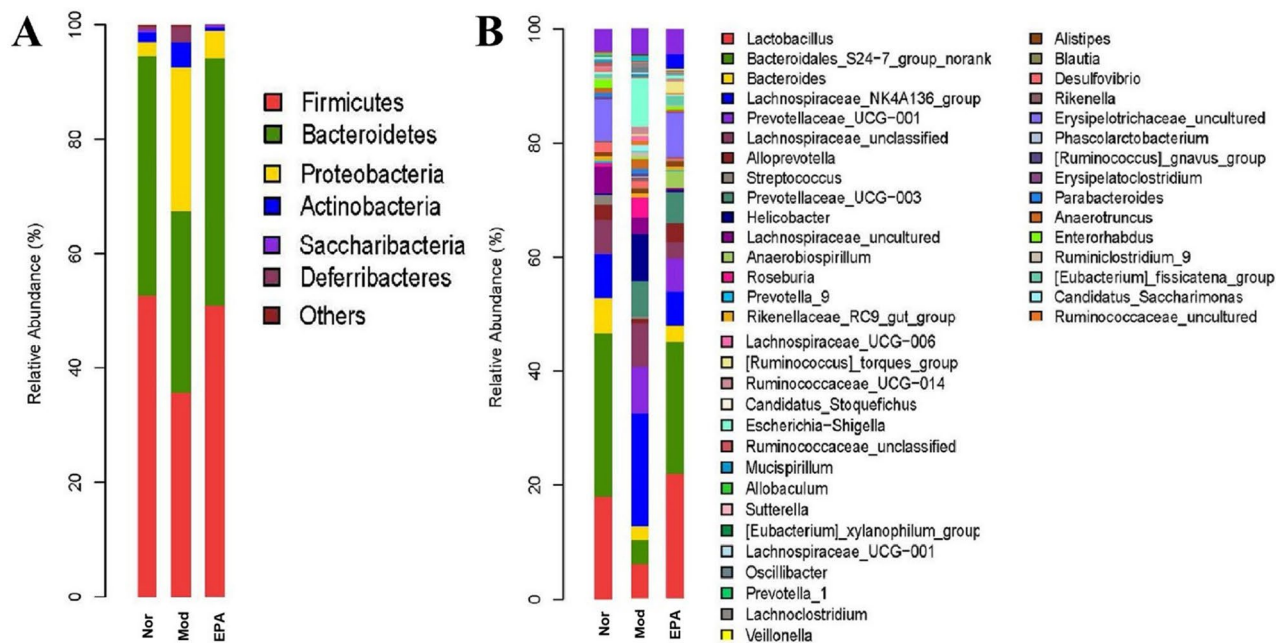


Figure 15. Taxonomic profiles of the fecal bacteria in the four groups at the phylum level (a) and genus level (b).

Abundance (%)			
	A	B	C
<i>Firmicutes</i>	53.63254	38.56821	51.84526
<i>Bacteroidetes</i>	37.78549	31.18542	39.85831
<i>Proteobacteria</i>	3.37934	24.44789	7.15324
Total	94.79737	94.20152	98.85681

Table 3. The relative abundance of the main gut microbiota at the phylum level in four groups.

normal group, the abundance of beneficial microflora such as *Lactobacillus*, *Bacteroidales_S24-7_group_norank*, *Bacteroidales*, *Alloprevotella* and *Alistipes* in the model group decreased by 6.95%, 25.25%, 4.67%, 2.65%, and 0.68%, respectively; accordingly, compared with those in the model group, those in the EPA group increased by 10.67%, 19.94%, 1.34%, and 3.29%, respectively, which showed a significant reversion in the reduction in beneficial microflora in the model group. In contrast, compared with that in the normal group, the abundance of the harmful microflora *Lachnospiraceae_NK4A136_group*, *Prevotellaceae_UCG-001*, *Helicobacter*, and *Prevotellaceae_UCG-003* in the model group increased to 16.39%, 7.01%, 5.83%, and 8.81%, respectively, while those in the EPA-treated group decreased to 17.99%, 1.44%, 5.81%, and 3.33%, respectively. These results showed that EPA treatment balanced the relative abundance of beneficial and detrimental bacteria in the gut microflora, as observed in the normal group.

Discussion

The antitumor effect of EPA. Chemotherapy is an important cancer treatment, but it has side effects and high toxicity, which may be harmful to the body. In this study, although CTX had the highest TIR (92.42%), it seemed to damage the spleen and thymus, according to the organ index data. Additionally, the AST and BUN levels of the CTX-treated group were significantly increased, as seen by ELISA, thereby increasing the burden on the kidney and liver²⁶.

EPA is mainly composed of ergosterol, ergosterol peroxide, ergosta-4, 6, 8(14), 22-tetraen-3-one, and (22E, 24R)-ergosta-7, 22-dien-3 β , 5 α , and 6 β -triol. This study revealed that EPA had a relatively better antitumor effect and had an obvious protective effect on the liver, kidney, spleen, and thymus compared with CTX treatment. The ELISA results showed that EPA may have an inflammatory response that improves IL-2, IL-6, and IFN- γ levels in the serum to enhance immunity²⁷. H&E and TUNEL staining were performed to observe apoptosis in tumor cells and showed the remarkable antitumor efficacy of EPA in H22 tumor-bearing mice was mediated by inducing cell death/apoptosis.

The mitochondria-dependent pathway is one of the classic apoptosis pathways, and the most important players are members of the Bcl-2 family²⁸. A decrease in the ratio of Bcl-2 to BAX could determine the expression of apoptotic proteins in related tissues³⁰. After treatment with EPA, BAX expression increased significantly.

Abundance (%)			
	A	B	C
<i>Lactobacillus</i>	18.075844	11.127102	21.798470
<i>Bacteroidales_S24-7_group_norank</i>	28.471373	3.206927	23.148881
<i>Bacteroides</i>	6.387470	1.717157	3.058214
<i>Alloprevotella</i>	2.667242	0.0959440	3.305270
<i>Alistipes</i>	0.702790	0.021587	0.981027
<i>Lachnospiraceae_NK4A136_group</i>	7.593965	23.98599	5.994099
<i>Prevotellaceae_UCG-001</i>	0.018469	7.195798	5.754240
<i>Helicobacter</i>	0.287832	6.115133	0.314217
<i>Prevotellaceae_UCG-003</i>	0	8.807656	5.473603
Total	64.204985	62.273294	69.828021

Table 4. The relative abundance of the main gut microbiota at the genus level in four groups.

Bcl-2 expression and the ratio of Bcl-2 to BAX decreased. The immunohistochemical and western blot analyses results were consistent. Moreover, previous studies have reported that TNF- α levels could significantly increase the gene expression of BAX and decrease the gene expression of Bcl-2 in human tumor cells²⁹; these results were consistent with the ELISA results for TNF- α in this study. Cleaved Caspase 3 is a key apoptotic protein, and its presence indicated that apoptosis had occurred in the tumor cells in this study³⁰. Furthermore, cleaved caspase-3 levels significantly increased after EPA treatment. Therefore, we considered that the antitumor mechanism of EPA involves regulating the expression of Bcl-2 and BAX and activating the caspase family of proteins.

VEGF is a tumor marker and an important growth factor implicated in tumor angiogenesis³¹. In this study, after treatment with EPA, VEGF expression was obviously decreased. The immunohistochemical, ELISA, western blot, and RT-PCR results confirmed that EPA could effectively reduce tumor angiogenesis, promote the expression of apoptotic genes and proteins, and inhibit tumor growth.

Influence on the gut microbiota of mice. In this study, the gut microbiota in mice and the relative abundance of the main genera were analyzed. It was suggested that EPA could increase the abundance of beneficial microflora, decrease harmful microflora and restore the gut microbiota of tumor-bearing mice. The main harmful microbiota identified in this study included *Prevotella*, *Lachnospiraceae*, and *Helicobacter*.

Prevotella is a harmful organism and a common conditional pathogen that can cause dose-dependent visceral hypersensitivity and endogenous infections in some parts of the body. Both *Lachnospiraceae_NK4A136_group* and *Helicobacter* are classified as gram-negative anaerobic bacteria that can cause severe inflammation, such as diarrhea, watery stools, intestinal infections, bacteriosis, septicemia, cancer, and cholecystitis, and can cause immune dysfunction, bacterial flora imbalance, and endogenous infection³². The abundances of *Prevotella*, *Lachnospiraceae_NK4A136_group*, and *Helicobacter* were 0.02%, 7.59%, and 0.29%, respectively, in the normal group; 16.01%, 23.99%, and 6.12, respectively, in the model group; and 11.23%, 5.99%, and 0.31%, respectively, in the EPA-treated group (Fig. 15 and Table 4). This finding indicated that compared with physiological conditions, the tumor microenvironment can cause an endogenous infection and have an adverse effect on the structure of gut microbiota in mice. However, after treatment with EPA, *Prevotella*, *Lachnospiraceae_NK4A136_group*, and *Helicobacter* in tumor-bearing mice were significantly reduced and tended to be closer to the levels in the normal group.

The main beneficial microbiota included *Lactobacillus*, *Bacteroidales*, *Alloprevotella*, and *Alistipes*. *Lactobacillus* is a gram-positive bacterium that regulates the gut microflora, enhances immunity, protects the gastric mucosa, improves intestinal function, prevents diarrhea, promotes digestion and exerts antitumor and antioxidant effects^{33,34}. This organism breaks down polysaccharides for other bacteria in the intestine and plays an important role in intestinal balance³⁵.

Bacteroides and *Alistipes* belong to the genus Bacteria. *Bacteroides* is a symbiotic bacterium in the gut of humans that provides essential nutrients and directly inhibits the adhesion and invasion of other harmful bacteria through their own colonization³⁶. According to reports, *Bacteroides* and its metabolites are closely related to tumors and can regulate cell proliferation, differentiation, and apoptosis and inhibit tumors³⁷. *Alistipes* is a relatively new genus that is highly associated with dysbiosis and disease³⁸. This genus also has protective effects against some diseases, such as cancer, liver fibrosis, colitis and cardiovascular disease³⁹. In this study, EPA effectively reduced tumor angiogenesis and promoted the expression of apoptotic genes and proteins, such as BAX, Bcl-2, VEGF, and cleaved caspase 3. Thus, we can conclude that the antitumor effect of EPA may be related to beneficial microbiota *Bacteroides* and some antitumor or apoptosis pathways.

Alloprevotella has the ability to produce folic acid and vitamin B1, which are important bioactive substances that are decomposed and utilize proteins in the intestinal mucosa⁴⁰. The final metabolites are succinic acid and acetic acid. It has been reported that appropriate proportions of succinic acid and acetic acid can directly provide energy for the intestinal epithelium, improve intestinal digestion and absorption of nutrients, and improve intestinal immunity⁴¹.

Conclusions and expectation

According to the literature, extracts of edible and medicinal fungi have anti-inflammatory effects and reduce the release of cytokines⁴². In a previous study, polysaccharides were extracted from *Pholiota adiposa*, which inhibited tumors⁸. In this study, we concluded that EPA could significantly increase the TIR, especially in the HD group of EPA-treated mice, which was the positive treatment group (CTX). Verification of the molecular mechanism after treatment with EPA by immunohistochemical, ELISA, western blot, and RT-PCR assays showed that EPA could effectively reduce tumor angiogenesis, promote the expression of apoptotic genes and proteins, and inhibit tumor growth.

Instability in the gut microbiota is one of the causes of cancer⁴³. Dysbacteriosis may make an individual prone to chronic inflammation, and chronic inflammation increases the risk of developing tumors⁴⁴. At present, the possible correlation between the gut microbiota and tumors has been studied. The gut microbiota also has an impact on the generation, development, therapeutic efficacy, and treatment of malignant tumors⁴⁵.

In this study, harmful microbiota were increased, while beneficial microbiota were decreased in mice inoculated with H22 hepatoma cells. After treatment with EPA, the gut microbiota of tumor-bearing mice tended to be closer to that of normal mice. Hence, EPA may increase the abundance of beneficial microbiota and decrease the abundance of harmful microbiota. The findings of our study provide data for future research on disease and microecology.

In conclusion, although EPA can regulate the gut microbiota of tumor-bearing mice, the specific mechanism remains unclear. With the development of macrogenomics, metabonomics, and molecular biology, researchers will have a more specific understanding of the interaction between food or drugs and the gut microbiota. This study will further deepen and expand research on EPA, its antitumor mechanism, and its influence on the gut microbiota.

Methods and materials

Materials and equipment. The fruits of *P. adiposa* were purchased from Mushroom professional cooperative in Songyuan, Songyuan City, Changchun, China, which cultivate a variety of edible and medicinal mushroom, such as *Pholiota adiposa*, *Pholiota microspora*, *Pleurotus eryngii*, and *Pleurotus ostreatus* et al. In this study, the sample of *P. adiposa* were identified by Professor Tolgor Bau of Jilin Agricultural University, who is a famous taxonomist in China. And the voucher specimen of *P. adiposa* was deposited in the Fungus herbarium of Jilin Agricultural University which is a publicly available herbarium (Specimen Number, JLAU28202). In this study, the collection of *P. adiposa*, complied with relevant institutional, national, and international guidelines and legislation.

All other chemical reagents used in this study were analytical grade. The Cyclophosphamide (CTX) for injection was purchased from Shanghai Huili Biotechnology Co., Ltd. Hematoxylin and Eosin (H&E) dye kits were obtained from Nanjing Jiancheng Bioengineering Research Institute (Nanjing, China). TUNEL assay was performed in situ by using the apoptosis detection kit (Roche, Branchburg, NJ, USA) and the DAB detection kit. ELISA kits for mouse, include Interferon- γ (IFN- γ), Interleukin-2 (IL-2), Interleukin-6 (IL-6), Tumor Necrosis Factor- α (TNF- α), and vascular endothelial growth factor (VEGF) ELISA kits were purchased from American R&D Co., Ltd. (Minneapolis, MN, USA). Rabbit polyclonal antibodies against Bcl-2(3498S), Bax(2772S), Caspase3 (9661 s), and mouse monoclonal VEGF(AV202) antibody were purchased from Cell Signaling Technology (Danvers, MA, USA). TripleTOF 5600 + LC/MS/MS (AB SCIEX, America). Agilent 1290 Infinity LC/MS (Agilent, America). 95% ethanol was purchased from Nanjing Chemical Reagents Co., Ltd. (Nanjing, China); acetonitrile, methanol and acetone were purchased from Merck Company (chromatographic grade, Merck Company of Germany). Real-time PCR detector (LC96, Swiss).

Preparation and LC-MS analysis of *P. adiposa* extracts (EPA). Briefly, dried and powdered of *P. adiposa* (1000 g) was extracted with 75% aqueous EtOH by ultrasonic treatment. The ultrasound conditions were ultrasonic power of 500 W, ultrasonic temperature of 60 °C, ethanol concentration of 75%, liquid to solid ratio of 37:1 and extraction time of 32 min. Then, EPA was concentrated, freeze-dried. The final crude extract (66.42 g) was stored at -20 °C for further use.

For LC-MS analysis, 10 mg of EPA was dissolved in 5 ml of formic acid ultra-pure water solution and was filtered through 0.22 μ m nylon membrane before LC-MS analysis. Ultrasonic extraction method was used to extract at 60°C for 30 min, repeated 3 times, centrifuged at 10 000r/min for 5 min, combined with supernatant and sample analysis. The Waters ACQUITY UPLC BEH C18 (100 mm \times 2.1 mm, 1.7 μ m) column was used for chromatographic analysis in gradient elution mode at the flow rate of 0.3 mL/min and column temperature of 40°C. The mobile phase A was set as ultra-pure water containing 0.1% formic acid, and mobile phase B is acetonitrile, flow rate: 0.3 mL/min, and gradient elution mode is used for chromatographic separation (Table 5). Ionization mode Qualitative analysis mass spectrometry conditions: electrospray ionization (ESI); Negative ion mode and MSE mode were used for full scan analysis. Ion scanning range: m/z 50 ~ 2000; The temperature of dissolution is 400°C, the flow rate of dissolution gas is 800L/h; Low energy voltage: 6 eV; High energy voltage 20-50 eV; Ion source temperature: 120°C, capillary voltage: 2.5 kV. After then, UPLC-QTOF-MSE mode was used to collect data, and Waters UNIFI software was used to analyze the results.

Antitumor activity in vivo. *Animals and cell lines.* Specific Pathogen Free grade, 6–8 week old male ICR mice that weighted at 20 \pm 2 g, were purchased from Liaoning Changsheng Biotechnology Co., Ltd. (Liaoning, China), with Certificate No.: SCXK (Liao) 2019-0001. The mice were supplied with standard laboratory diet and water ad libitum at a temperature 25 \pm 2 °C with a 12-h light/ dark cycle (lights on 8:00 AM to 8:00 PM) and all mice were adapted to the environment for one week. And all experimental procedures were strictly in accord-

Time(min)	Mobile Phase	
	A(%)	B(%)
0	95	5
2	80	5
5	50	20
15	20	50
45	10	95
55	10	95
55.01	95	5
65	95	5

Table 5. LC/MS-Q-TOF gradient elution program.

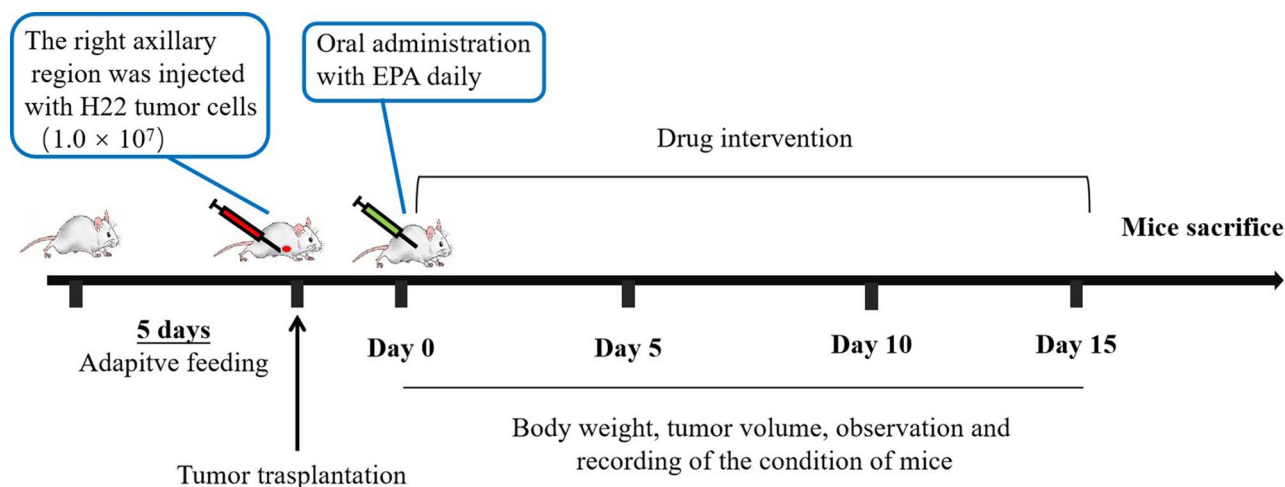


Figure 16. Anti-tumor experimental design scheme of H22 in vivo.

ance with the Regulations of Experimental Animal Administration issued by the Ethical Committee for Laboratory Animals at Jilin Agricultural University (Permit No. ECLA-JLAU-19036). And I confirm that all methods are reported in accordance with ARRIVE guidelines for the reporting of animal experiments.

The mouse H22-hepatoma cell line was purchased from Jilin Provincial Cancer Hospital (Jilin, China). H22 tumor mice were prepared as described previously, which were maintained in the ascitic form by sequential passages into the peritoneal cavities of male ICR mice⁴⁶.

Preparation of tumor-bearing mice and treatment protocol. The H22-hepatoma cells was prepared with concentration of 1.0×10^7 cells/mL. All mice except normal group were inoculated in the subcutaneous right forelimb armpit with the tumor cell suspension (0.1 mL for each mice) to establish the tumor-bearing mice model. 24 h later, 10 mice in each group were randomly divided into five groups (The experimental design is shown in Fig. 16) and each 5 mice were in one caged. The tumor-bearing mice were defined as the model group, the positive treatment group and the EPA treatment group, of which the EPA treatment group was further divided into high, medium and low dose groups, the doses of which were 300 mg/kg (HD), 200 mg/kg (MD) and 100 mg/kg (LD) respectively. The control mice were given the same volume of saline solution intragastrically and the positive control were intraperitoneally injected with 25 mg/kg CTX. All groups of mice were treated 1 time/d for 14 days. After then, all mice were killed by euthanasia and the tumor tissues were excised and weighted. The index of tumor inhibition rate (TIR) was calculated as $100\% \times (\text{average tumor weight of the control group} - \text{average tumor weight of the treatment group}) / \text{average tumor weight of the control group}$. The derivative with the highest TIR continued to be subjected to subsequent experiments.

Determination of biochemical parameters. Freshly heparinized blood was prepared from orbital venous plexus of the mice. After being centrifuged at 1500 rpm for 20 min at 4 °C, sera were collected and the serum samples of all groups were kept 4 °C for biochemical assay. In accordance with the procedures described in the commercial kit, AST, BUN, IL-2, IL-6, TNF- α , IFN- γ and VEGF levels of the mice were determined by indirect ELISA assay⁴⁷.

Primer	Sequence(5'-3')
Caspase3-F	GCGACTACTGCCGGAGTCT
Caspase3-R	ACCGGTATCTTCTGGCAAGC
BAX-F	GGTTGCCCTCTTCTACTTTGC
BAX-R	GTCCAGCCCATGATGGTTCT
BCL2-F	CTCTCGTCGCTACCGTCGT
BCL2-R	CCGAAGTCAAAGAAGGCCAC
VEGF-A-F	TACTGCCGTCGGATTGAGAC
VEGF-A-R	TCCAGGGCTTCATCGTTACA

Table 6. Primers used in the present study.

H & E and TUNEL assay. The H&E staining of H22 solid tumor cells were conducted following the manufacturer's instructions in respective kit, and their results were obtained by optical microscope, and the H & E staining results of the tumor was shown as color images at 400× magnification⁴⁸. TUNEL assay method was used to detect apoptotic cells in tumor tissues⁴⁹. The tumor tissue sections were treated with 20 mg/mL of proteinase K distilled water for 15 min at room temperature. After that, 50 μL TUNEL solution was added and incubated in the kit at 37°C for 60 min. Peroxidase activity in each tissue section was indicated by applying diaminobenzidine.

Immunohistochemistry. The tumor tissue was fixed in 10% formaldehyde solution for 24 h, then decolorized and buried. After then the tumor tissue were cut into 4-micron slices for immunohistochemical staining which was performed using a murine/rabbit IgG immunohistochemistry kit (VEGF, Bcl-2, BAX, caspase3). Tumor tissue growth and apoptosis were evaluated by cell sequence, size of necrotic area, positive cell count and staining intensity score⁵⁰.

Western blot assay and quantitative real-time PCR. The method of western blotting was used for qualitative and quantitative analysis of proteins⁵¹. Cell lysates were prepared, after then, concentrations of total protein were measured using a BCA assay kit (Pierce, Rockford, IL). Then, the total protein in some tumor tissues was extracted and the protein content of each cell sample was determined by coomassant bright blue method⁵². All proteins were resolved on a 15% SDS-denaturing polyacrylamide gel and then transferred onto a polyvinylidene fluoride (PVDF) membrane. The membranes were incubated with antibodies against Bax(1:1000), caspase3(1:1000), Bcl-2(1:1000), and VEGF(1:1000) overnight at 4 °C. The membrane was then washed in PBST and incubated with horseradish peroxidase-conjugated sheep anti-rabbit (1:3000) and equine anti-mouse at room temperature for 1 h. And finally, the enhanced chemiluminescence (ECL) reagent was added and protein mildness was observed by enhanced chemiluminescence detection system (Amersham Pharmacia Biotechnology, Tokyo, Japan). This method was used to analyze the levels of antiapoptotic factor Bcl-2, BAX, VEGF, and Caspase3.

The method of RT-PCR was carried out as described previously⁵³. Using Trizol reagent to isolate the total RNA from the tumor tissue, then reverse transcribed into cDNA. And each cDNA sample was tested using a real-time SYBR Green PCR reagent with specific primers (Table 6). The mRNA expression levels of Bcl-2 (3498S), Bax (2772S), Caspase3 (9661 s), VEGF (AV202) and β-actin were calculated by 2^{-ΔΔct} method and expressed as a ratio compared to control.

DNA extraction and 16 s rDNA high-throughput sequencing. *Collection and preparation of blood samples.* Normal group, model group and HD of EPA (300 mg/kg) group were tested, and QIAamp Fast DNA Stool Kit (50) (Qiagen, Hamburg, Germany) was used to extract the DNA from the feces of the mice. A KAPA HiFi Hotstart ReadyMix PCR Kit was used for the PCR analysis. Using bar-coded primers 341F (5'-CCTAYG GGRBGCASCAG-3') and 806R (5'-GGACTACNNGGGTATCTAAT-3') to amplify the V3-V4 hypervariable regions of bacterial 16 s rDNA (from 341 to 806) from the extracted DNA, after then, the fluorimeter Qubit3.0 were used to pool, purify and quantify the amplicons⁵⁴. The amplicons were purified and quantified before being sequenced on the HiSeq 2500 PE250 Amplifier sequencing platform (Illumina, San Diego, CA, USA) by a commercial company (BIOPROFILE TECHNOLOGY Technology Co. Ltd., SHANGHAI, China).

Statistical analysis. All data were presented as the mean ± standard deviation (S.D.). The significance of the differences was determined by a one-way analysis of variance (ANOVA) followed by the Duncan's test, with a p < 0.05 considered to be significant. Statistical analyses were performed using SPSS version 19.0.

Paired-End sequencing were obtained from Illumina PE250 sequencing. Paired-End Reads grow Reads through the Overlap relationship between Reads, and quality control of the spliced Reads. After then, get the Clean Reads. According to overlap, sequence quality is controlled and filtered. OTU cluster analysis (Operational Taxonomic Units) and taxonomic analysis were performed after sample distinguished. Finally, all Clean Reads are compared to OTU, and the Reads of OTU that can be compared are extracted. Get the final apped Reads.

In this research, alpha diversity index analysis method, which reflect the abundance and diversity of microbial communities, was used to analysis the single sample diversity which reflect the abundance and diversity

of microbial communities. The diversity of gut bacteria were calculated by Shannon index, Simpson index and PD whole tree index, and abundance of bacteria calculate were calculated by the observed species index and Chao1 index. Beta diversity reflects the differences among different grouping samples. Anosim analysis, PCoA analysis, LefSe difference analysis, rank between groups and other methods were used to analyze the difference significance.

Received: 12 November 2021; Accepted: 6 April 2022

Published online: 21 May 2022

References

- Jin, D., He, J., Luo, X. & Zhang, T. Hypoglycemic effect of Hypericum attenuatum Choisy extracts on type 2 diabetes by regulating glucolipid metabolism and modulating gut microbiota. *J. Funct. Foods* **52**, 479–491. <https://doi.org/10.1016/j.jff.2018.11.031> (2019).
- Jaeger, J. A. G., Raumer, H.-G.-V., Esswein, H., Müller, M. & Schmidt-Lüttmann, M. Time series of landscape fragmentation caused by transportation infrastructure and urban development: A case study from Baden-Württemberg, Germany. *Ecol. Soc.* **12**(1), 1288–1298. <https://doi.org/10.0000/PMID22> (2007).
- Zhang, Y. *et al.* A novel antitumor protein from the mushroom *Pholiota nameko* induces apoptosis of human breast adenocarcinoma MCF-7 cells in vivo and modulates cytokine secretion in mice bearing MCF-7 xenografts. *Int. J. Biol. Macromol.* **164**, 3171–3178. <https://doi.org/10.1016/j.ijbiomac.2020.08.187> (2020).
- Chen, F. *et al.* Antitumor and immunomodulatory effects of ginsenoside Rh2 and its octyl ester derivative in H22 tumor-bearing mice. *J. Funct. Foods* **32**, 382–390. <https://doi.org/10.1016/j.jff.2017.03.013> (2017).
- Yan, L. *et al.* Structural characterization and in vitro antitumor activity of A polysaccharide from *Artemisia annua* L. (Huang Huahao). *Carbohydr. Polym.* **213**, 361–369. <https://doi.org/10.1016/j.carbpol.2019.02.081> (2019).
- Ning, C. *et al.* Chicory inulin ameliorates type 2 diabetes mellitus and suppresses JNK and MAPK pathways in vivo and in vitro. *Mol. Nutr. Food Res.* **61**(8), 1600673. <https://doi.org/10.1002/mnfr.201600673> (2017).
- Jatuwong, K., Kumla, J., Suwannarach, N., Matsui, K. & Lumyong, S. Bioprocessing of agricultural residues as substrates and optimal conditions for phytase production of chestnut mushroom, *Pholiota adiposa*, in solid state fermentation. *J. Fungi* **6**, 384. <https://doi.org/10.3390/jof6040384> (2020).
- Zou, Y., Fang, Du., Qingxiu, Hu. & Wang, H. The structural characterization of a polysaccharide exhibiting antitumor effect from *Pholiota adiposa* mycelia. *Sci. Rep.* **9**(1), 1724–1733. <https://doi.org/10.1038/s41598-018-38251-6> (2019).
- Qi, H. *et al.* Dietary recombinant phycoerythrin modulates the gut microbiota of H22 tumor-bearing mice. *Mar. Drugs* **17**(12), 665. <https://doi.org/10.3390/md17120665> (2019).
- Wang, X., Bao, H. & Bau, T. Investigation of the possible mechanism of two kinds of sterols extracted from *Leucocalocybe mongolica* in inducing HepG2 cell apoptosis and exerting anti-tumor effects in H22 tumor-bearing mice. *Steroids* **163**, 108692. <https://doi.org/10.1016/j.steroids.2020.108692> (2020).
- Tracy, H. Gut microbes may shape response to cancer immunotherapy. *JAMA* **319**(5), 430–431. <https://doi.org/10.1001/jama.2017.12857> (2018).
- Chassaing, B. *et al.* Dietary emulsifiers impact the mouse gut microbiota promoting colitis and metabolic syndrome. *Nature* **519**(7541), 92–96. <https://doi.org/10.1038/nature14232> (2015).
- Kaiser, J. Gut microbes shape response to cancer immunotherapy. *Science* **358**(6363), 573–573. <https://doi.org/10.1126/science.358.6363.573> (2017).
- Ivana, B., Tobias, K., Jian, Ji. & Oliver, F. Software Tools and approaches for compound identification of LC-MS/MS data in metabolomics. *Metabolites* **8**(2), 31–53. <https://doi.org/10.3390/metabo8020031> (2018).
- Paula, B. *et al.* A new ESI-LC/MS approach for comprehensive metabolic profiling of phytocannabinoids in Cannabis. *Sci. Rep.* **8**(1), 14280. <https://doi.org/10.1038/s41598-018-32651-4> (2018).
- Lin, M. *et al.* 2-Naphthoic acid ergosterol ester, an ergosterol derivative, exhibits anti-tumor activity by promoting apoptosis and inhibiting angiogenesis. *Steroids* **122**, 9–15. <https://doi.org/10.1016/j.steroids.2017.03.007> (2017).
- Chen, Q., Yang, L., Han, M., Cai, E. & Zhao, Y. Synthesis and pharmacological activity evaluation of arctigenin monoester derivatives. *Biomed. Pharmacother.* **84**, 1792–1801. <https://doi.org/10.1016/j.biopha.2016.10.093> (2016).
- Lai, X., Xia, W., Wei, J. & Ding, X. Therapeutic effect of astragalus polysaccharides on hepatocellular carcinoma H22-bearing mice. *Dose-Response* **15**(1), 155932581668518. <https://doi.org/10.1177/1559325816685182> (2017).
- Bates, S. T. *et al.* Global biogeography of highly diverse protistan communities in soil. *The ISME J.* **7**(3), 652–659. <https://doi.org/10.1038/ismej.2012.147> (2013).
- Romay, Ch., Gonzalez, R., Ledon, N., Ramirez, D. & Rimbau, V. C-phycoyanin: A biliprotein with antioxidant, anti-inflammatory and neuroprotective effects. *Curr. Protein Pept. Sci.* **4**(3), 207–216. <https://doi.org/10.2174/1389203033487216> (2003).
- Zhang, Na. *et al.* Neogargarotetraose protects mice against exhaustive exercise-induced dyslipidemia by modulating gut microbial composition and function. *Food Sci.* **39**, 165–171 (2018).
- Maughan, H. *et al.* Analysis of the cystic fibrosis lung microbiota via serial Illumina sequencing of bacterial 16S rRNA hypervariable regions. *PLoS ONE* **7**(10), e45791. <https://doi.org/10.1371/journal.pone.0045791> (2017).
- Wang, J. *et al.* Metagenomic analysis of gut microbiota alteration in a mouse model exposed to mycotoxin deoxynivalenol. *Toxicol. Appl. Pharmacol.* **372**, 47–56. <https://doi.org/10.1016/j.taap.2019.04.009> (2019).
- Shaufi, M. A. M., Sieo, C. C., Chong, C. W., Gan, H. M. & Ho, Y. W. Deciphering chicken gut microbial dynamics based on high-throughput 16S rRNA metagenomics analyses. *Gut Pathogens* **7**(1), 4. <https://doi.org/10.1186/s13099-015-0051-7> (2015).
- Xiaofei, Xu. & Zhang, X. Effects of cyclophosphamide on immune system and gut microbiota in mice. *Microbiol. Res.* **171**, 97–106. <https://doi.org/10.1016/j.micres.2014.11.002> (2015).
- Jianfang, Fu. *et al.* Anti-diabetic activities of *Acanthopanax senticosus* polysaccharide (ASP) in combination with metformin[J]. *Int. J. Biol. Macromol.* **50**(3), 619–623. <https://doi.org/10.1016/j.ijbiomac.2012.01.034> (2012).
- Marcia, C. V. *et al.* 3,3',5,5'-tetramethoxybiphenyl-4,4'diol induces cell cycle arrest in G2/M phase and apoptosis in human non-small cell lung cancer A549 cells. *Chem. Biol. Interact.* **326**, 109133 (2020).
- Li, S. *et al.* ALLN hinders HCT116 tumor growth through Bax-dependent apoptosis. *Biochem. Biophys. Res. Commun.* **437**(2), 325–330. <https://doi.org/10.1016/j.bbrc.2013.06.088> (2013).
- Li, W. *et al.* Anti-tumor effect of steamed codonopsis lanceolata in h22 tumor-bearing mice and its possible mechanism. *Nutrients* **7**(10), 8294–8307. <https://doi.org/10.3390/nu7105395> (2015).
- Li, X., Bau, T. & Bao, H. FPOA induces apoptosis in HeLa human cervical cancer cells through a caspase-mediated pathway. *Oncol. Lett.* **15**(6), 8357–8362. <https://doi.org/10.3892/ol.2018.8380> (2018).
- Liu, B. *et al.* Triptolide downregulates treg cells and the level of IL-10, TGF- β , and VEGF in melanoma-bearing mice. *Planta Med.* **79**(15), 1401–1407. <https://doi.org/10.1055/s-0033-1350708> (2013).

32. Song, J. J. *et al.* Effects of microencapsulated *Lactobacillus plantarum* LIP-1 on the gut microbiota of hyperlipidaemic rats. *Br. J. Nutr.* **118**(7), 481–492. <https://doi.org/10.1017/S0007114517002380> (2017).
33. Segawa, S., Wakita, Y., Hirata, H. & Watari, J. Oral administration of heat-killed *Lactobacillus brevis* SBC8803 ameliorates alcoholic liver disease in ethanol-containing diet-fed C57BL/6N mice. *Int. J. Food Microbiol.* **128**(2), 371–377. <https://doi.org/10.1016/j.ijfoodmicro.2008.09.023> (2008).
34. Zhao, L. *et al.* Protective effects of *Lactobacillus plantarum* C88 on chronic ethanol-induced liver injury in mice. *J. Funct. Foods* **35**, 97–104. <https://doi.org/10.1016/j.jff.2017.05.017> (2017).
35. Suo, H. *et al.* *Lactobacillus fermentum* Suo Attenuates HCl/ethanol induced gastric injury in mice through its antioxidant effects. *Nutrients* **8**(3), 155–172. <https://doi.org/10.3390/nu8030155> (2016).
36. Zhang, Y. *et al.* Effects of shenling baizhu powder herbal formula on intestinal microbiota in high-fat diet-induced NAFLD rats. *Biomed. Pharmacother.* **102**, 1025–1036. <https://doi.org/10.1016/j.biopha.2018.03.158> (2018).
37. Patwardhan, G. A., Beverly, L. J. & Siskind, L. J. Sphingolipids and mitochondrial apoptosis. *J. Bioenerg. Biomembr.* **48**(2), 153–168. <https://doi.org/10.1007/s10863-015-9602-3> (2016).
38. Van den Abbeele, P. *et al.* Butyrate-producing Clostridium cluster XIVa species specifically colonize mucins in an in vitro gut model. *ISME J.* **7**(8), 949–961. <https://doi.org/10.1038/ismej.2012.158> (2013).
39. Parker, B. J., Wearsch, P. A., Veloo Alida, C. M. & Alex, R.-P. The genus *Alistipes*: Gut bacteria with emerging implications to inflammation, cancer, and mental health. *Front. Immunol.* **11**, 906. <https://doi.org/10.3389/fimmu.2020.00906> (2020).
40. Liew, W.-P.-P., Mohd-Redzwan, S. & Than, L. T. L. Gut Microbiota Profiling of Aflatoxin B1-Induced Rats Treated with *Lactobacillus casei* Shirota. *Toxins* **11**(1), 49. <https://doi.org/10.3390/toxins11010049> (2019).
41. Cheng, W. *et al.* Effect of Functional Oligosaccharides and Ordinary Dietary Fiber on Intestinal Microbiota Diversity. *Front. Microbiol.* **8**, 1750. <https://doi.org/10.3389/fmicb.2017.01750> (2017).
42. Zhao, Y. *et al.* UPLC-Q-TOF/HSMS/MS E⁻-based metabolomics for adenine-induced changes in metabolic profiles of rat faeces and intervention effects of ergosta-4,6,8(14),22-tetraen-3-one. *Chem. Biol. Interact.* **201**(1–3), 31–38. <https://doi.org/10.1016/j.cbi.2012.12.002> (2013).
43. Rutkowski, M. R. *et al.* Microbially driven TLR5-dependent signaling governs distal malignant progression through tumor-promoting inflammation. *Cancer Cell* **27**(1), 27–40. <https://doi.org/10.1016/j.ccell.2014.11.009> (2015).
44. Francesco, R. *et al.* Bile acids modulate tight junction structure and barrier function of Caco-2 monolayers via EGFR activation. *Am. J. Physiol.* **294**(4), G906–G913. <https://doi.org/10.1152/ajpgi.00043.2007> (2008).
45. Yoshimoto, S. *et al.* Obesity-induced gut microbial metabolite promotes liver cancer through senescence secretome. *Nature* **499**(7456), 97–101. <https://doi.org/10.1038/nature12347> (2013).
46. Wang, X., Bao, H. & Bau, T. Investigation of the possible mechanism of polysaccharides extracted from *Leucocalocybe mongolica* in exerting antitumor effects in H22 tumor-bearing mice. *J. Food Biochem.* **45**(4), e13514. <https://doi.org/10.1111/JFBC.13514> (2021).
47. Deng, X. *et al.* Antitumor activity of *Lycium barbarum* polysaccharides with different molecular weights: An in vitro and in vivo study. *Food Nutr. Res.* **61**(1), 1399770. <https://doi.org/10.1080/16546628.2017.1399770> (2017).
48. Yang, B., Xiao, B. & Sun, T. Antitumor and immunomodulatory activity of *Astragalus membranaceus* polysaccharides in H22 tumor-bearing mice. *Int. J. Biol. Macromol.* **62**(11), 287–290. <https://doi.org/10.1016/j.ijbiomac.2013.09.016> (2013).
49. Ni, C. *et al.* IFN- γ selectively exerts pro-apoptotic effects on tumor-initiating label-retaining colon cancer cells. *Cancer Lett.* **336**(1), 174–184. <https://doi.org/10.1016/j.canlet.2013.04.029> (2013).
50. Wang, T. *et al.* Enhanced tumor delivery and antitumor activity in vivo of liposomal doxorubicin modified with MCF-7-specific phage fusion protein. *Nanomedicine* **10**(2), 421–430 (2014).
51. Han, C. *et al.* *Salvia miltiorrhiza* polysaccharides protect against lipopolysaccharide-induced liver injury by regulating NF- κ B and Nr1f2 pathway in mice. *Food Hydrocolloids* **30**(1), 979–994. <https://doi.org/10.1080/09540105.2019.1652250> (2019).
52. Zhao, X., Ma, S., Liu, N., Liu, J. & Wang, W. A polysaccharide from *Trametes robiniophila* inhibits human osteosarcoma xenograft tumor growth in vivo. *Carbohydr. Polym.* **124**, 157–163. <https://doi.org/10.1016/j.carbpol.2015.02.016> (2015).
53. Yang, J., Li, X., Xue, Y., Wang, N. & Liu, W. Anti-hepatoma activity and mechanism of corn silk polysaccharides in H22 tumor-bearing mice. *Int. J. Biol. Macromol.* **64**, 276–280. <https://doi.org/10.1016/j.ijbiomac.2013.11.033> (2014).
54. Ren, F., Qian, X. & Qian, X. *Astragalus* polysaccharide upregulates hepcidin and reduces iron overload in mice via activation of p38 mitogen-activated protein kinase. *Biochem. Biophys. Res. Commun.* **472**(1), 163–168. <https://doi.org/10.1016/j.bbrc.2016.02.088> (2016).
55. Tomoya, Y., Takuo, E., Naoto, S. & Ken-ichi, H. Gut microbiota and coronary artery disease. *Int Heart J* **57**(6), 663–671. <https://doi.org/10.1536/ihj.16-414> (2016).
56. Shang, Q. *et al.* Dietary Polysaccharide from *Enteromorpha Clathrata* Modulates Gut Microbiota and Promotes the Growth of *Akkermansia muciniphila*, *Bifidobacterium* spp and *Lactobacillus* spp. *Mar. Drugs* **16**(5), 167–182. <https://doi.org/10.3390/md16050167> (2018).

Acknowledgements

The authors are grateful for the National Natural Science Foundation of China (grant No. 31870014). We declare that there are no financial or other contractual agreements that might cause conflicts of interest or be perceived as causing conflicts of interest.

Author contributions

X.W.: Conceptualization, Data curation, Formal analysis, Investigation, Resources, Software, Visualization, Writing-original draft. Y.Z.: Formal analysis, Methodology, Resources, Validation, Writing-review & editing. F.L.: Conceptualization, Data curation, Formal analysis, Funding acquisition, Investigation, Methodology, Project administration, Resources, Software, Supervision, Validation, Visualization, Writing-original draft, Writing-review & editing.

Competing interests

The authors declare no competing interests.

Additional information

Supplementary Information The online version contains supplementary material available at <https://doi.org/10.1038/s41598-022-11041-x>.

Correspondence and requests for materials should be addressed to F.L.

Reprints and permissions information is available at www.nature.com/reprints.

Publisher's note Springer Nature remains neutral with regard to jurisdictional claims in published maps and institutional affiliations.



Open Access This article is licensed under a Creative Commons Attribution 4.0 International License, which permits use, sharing, adaptation, distribution and reproduction in any medium or format, as long as you give appropriate credit to the original author(s) and the source, provide a link to the Creative Commons licence, and indicate if changes were made. The images or other third party material in this article are included in the article's Creative Commons licence, unless indicated otherwise in a credit line to the material. If material is not included in the article's Creative Commons licence and your intended use is not permitted by statutory regulation or exceeds the permitted use, you will need to obtain permission directly from the copyright holder. To view a copy of this licence, visit <http://creativecommons.org/licenses/by/4.0/>.

© The Author(s) 2022